Applied Catalysis B: Environmental 96 (2010) 350–360

Contents lists available at ScienceDirect

Applied Catalysis B: Environmental

journal homepage: www.elsevier.com/locate/apcatb

Effects of Ce/Zr ratio on the reducibility, adsorption and catalytic activity of $CuO/Ce_xZr_{1-x}O_2/\gamma$-$Al_2O_3$ catalysts for NO reduction by CO

Qiang Yu[a], Lianjun Liu[a], Lihui Dong[a], Dan Li[a], Bin Liu[a], Fei Gao[b,*], Keqin Sun[c], Lin Dong[a,b,**], Yi Chen[a]

[a] Key Laboratory of Mesoscopic Chemistry of Ministry of Education, School of Chemistry and Chemical Engineering, Nanjing University, Nanjing 210093, PR China
[b] Center of Modern Analysis, Nanjing University, Nanjing 210093, PR China
[c] School of Energy and Environment, Southeast University, Nanjing 211102, PR China

ARTICLE INFO

Article history:
Received 10 November 2009
Received in revised form 4 February 2010
Accepted 24 February 2010
Available online 3 March 2010

Keywords:
$CuO/Ce_xZr_{1-x}O_2/\gamma$-$Al_2O_3$
NO + CO model reaction
H_2-TPR
In situ FT-IR
Carbonate
Nitrate

ABSTRACT

Effects of Ce/Zr ratio on the physicochemical properties of $CuO/Ce_xZr_{1-x}O_2/\gamma$-$Al_2O_3$ catalysts were investigated by BET, XRD, Raman and H_2-TPR. The catalytic activity and the interaction between the reactants with these catalysts were compared by NO + CO model reaction and in situ FT-IR. The results suggested that the addition of ceria–zirconia mixed oxides significantly improved NO conversion and N_2 yield due to dispersed copper species in proximity to ceria–zirconia. Especially, the ceria-rich catalysts displayed better performance in activity and reducibility than others, which would be resulted from the strong interaction among copper, ceria–zirconia and support. The IR results suggested NO reduction activity was correlated with the presence of Cu^+ carbonyl species, and the catalysts with variable Ce/Zr ratios had no distinction at the adsorption type and rate of NO/CO at room temperature. However, on heating treatment would give distinct difference in CO_2 intensity and the wavenumber of adsorbed nitrates. Simultaneously, the stability of these N- and C-containing intermediates contacted with alumina was influenced by the modified Ce/Zr ratio.

1. Introduction

The catalytic reduction of NO by CO without the presence of O_2, H_2O and CO_2 was an appropriate model reaction, which was different with real automobile exhaust emission. However, amounts of fundamental studies using the supported noble metal catalysts were carried out to expect to approach the nature of this reaction [1–6]. Moreover, many efforts have been devoted to employing the potential substitute as active component of the three-way catalysts (TWCs) due to the scarcity and high cost of noble metal. For example, it was found that CuO/γ-Al_2O_3 system attracted much attention for the removal of NO with CO because of its promising catalytic activity and thermal stability [7–13]. Nevertheless, it still showed the unsatisfactory activity and selectivity for NO reduction at low temperature. Therefore, many studies were performed to improve its efficiency and stability by introducing other promoters, such as ceria [14–18], lanthana [19], yttria-doped ceria (YDC) [20], samaria-doped ceria (SDC) [21], and zirconia [22,23], etc. Among them, ceria–zirconia exhibited the extraordinary effect on the catalytic activity of CuO/γ-Al_2O_3 system, which has been considered as the effective and crucial components for the commercial TWCs [24]. This was due to its outstanding oxygen storage capacity and redox properties [25–27]. On the other hand, it was documented that there was a synergic stabilization effect between ceria–zirconia mixed oxides and alumina, which can further retard the sintering of ceria–zirconia by the presence of alumina, particularly at high zirconia content [28]. Meanwhile, the phase transformation of γ-Al_2O_3 was hindered by the presence of ceria and zirconia.

More recently, Martínez-Arias et al. [29] found that Pd interacting with dispersed ceria–zirconia promoter species resulted in the higher NO reduction for Pd-based catalysts under stoichiometric CO + NO + O_2 model gas. Moreover, the extent of promotion effect of ceria–zirconia depends on the interaction between metal and support. Along this line, it was expected that combining the advantages of CuO/γ-Al_2O_3 system and ceria–zirconia mixed oxides promoter to achieve the goal of high reactivity and low cost. It should be pointed out that these previous studies focused on its bulk structure and properties at high content of ceria–zirconia with a fixed Ce/Zr ratio [30]. Limited attention was paid to the low loading of ceria–zirconia with variable Ce/Zr ratios as the modifier, and their dispersion and adsorption behaviors on the surface of γ-Al_2O_3 were not clear. Furthermore, the topic about the interaction among the copper species, ceria–zirconia with different Ce/Zr ratios and γ-Al_2O_3 support was still worthy of discussing, which would get

* Corresponding author at: Center of Modern Analysis, Nanjing University, Nanjing 210093, PR China. Tel.: +86 25 83592290; fax: +86 25 83317761.
** Corresponding author at: Key Laboratory of Mesoscopic Chemistry of Ministry of Education, School of Chemistry and Chemical Engineering, Center of Modern Analysis, Nanjing University, Nanjing 210093, PR China. Tel.: +86 25 83592290; fax: +86 25 83317761.
E-mail addresses: gaofei@nju.edu.cn (F. Gao), donglin@nju.edu.cn (L. Dong).

0926-3373/$ – see front matter © 2010 Elsevier B.V. All rights reserved.
doi:10.1016/j.apcatb.2010.02.032

insight into the influence on their reducibility and catalytic performance.

Based on our previous studies [31], the monolayer dispersion capacity of ceria on the γ-Al_2O_3 was nearly 0.1 mmol/100 m^2, and that for zirconia was 0.56 mmol/100 m^2. As a result, the total loading amount of ceria–zirconia was fixed at 0.1 mmol/100 m^2 γ-Al_2O_3 (about 2 wt%), which was much lower than the previous report [30]. The main objective of the present work was to explore the effects of Ce/Zr molar ratio on the reduction, adsorption, and catalytic activity of CuO supported on $Ce_xZr_{1-x}O_2$ modified γ-Al_2O_3 support. In situ FT-IR was also employed to investigate the interaction between the reactants and these catalysts with different Ce/Zr ratios by monitoring the vibration of NO_x and CO_x adsorbates.

2. Experimental

2.1. Catalyst preparation

2.1.1. $Ce_xZr_{1-x}O_2$/γ-Al_2O_3 supports

γ-Al_2O_3 was pre-calcined at 700 °C in air for 7 h. Its BET surface area was 156 m^2/g. Ceria–zirconia mixed oxides with different Ce/Zr ratios modified γ-Al_2O_3 was prepared by wet co-impregnating γ-Al_2O_3 with the requisite amounts of $(NH_4)_2Ce(NO_3)_6{\cdot}6H_2O$ and $Zr(NO_3)_4{\cdot}5H_2O$ solutions. The total amount of ceria–zirconia mixed oxides, i.e., Ce^{4+} and Zr^{4+} ions, was 0.1 mmol/100 m^2 γ-Al_2O_3. The molar ratio of Ce/Zr was 0:1, 1:2, 1:1, 2:1 and 1:0, respectively. The resultant solution was kept vigorous stirring for 1 h. After that, it was heated at 90 °C to vaporize the water. The supports were dried in air at 110 °C for 12 h and then calcined at 500 °C for 5 h. These as-prepared supports were denoted as ZA, $C_{0.33}Z_{0.67}A$, $C_{0.5}Z_{0.5}A$, $C_{0.67}Z_{0.33}A$ and CA, respectively. Additionally, considering the small quantity of ceria–zirconia addition, the BET surface area of $Ce_xZr_{1-x}O_2$/γ-Al_2O_3 supports ($C_xZ_{1-x}A$) are almost the same as that of γ-Al_2O_3.

2.1.2. CuO/$Ce_xZr_{1-x}O_2$/γ-Al_2O_3 catalysts

CuO-supported catalysts were prepared by wet impregnation of the above supports with a requisite amounts of $Cu(NO_3)_2{\cdot}3H_2O$ aqueous solution. The content of CuO was fixed at 0.4 mmol/100 m^2 γ-Al_2O_3. The obtained samples were dried at 110 °C overnight and then calcined at 500 °C in air for 5 h. These resultant catalysts were denoted as $04CuC_xZ_{1-x}A$, e.g., $04CuC_{0.33}Z_{0.67}A$ corresponds to the catalyst with a loading amount of 0.4 mmol CuO and 0.1 mmol ceria–zirconia mixed oxides with a Ce/Zr ratio of 1:2 on the 100 m^2 γ-Al_2O_3. In addition, 04CuO/γ-Al_2O_3 (denoted as 04CuA) reference catalyst was prepared following the similar procedure. The details for these catalysts were listed in Table 1.

2.2. Catalyst characterization

2.2.1. Brunauer–Emmet–Teller (BET)

BET surface area was measured by nitrogen adsorption at −196 °C on a Micrometrics ASAP-2020 adsorption apparatus. Prior to each measurement, the sample was degassed at 300 °C until a stable vacuum of ca. 10 μmHg was reached.

2.2.2. X-ray diffraction (XRD)

XRD patterns were recorded on a Philips X'Pert Pro diffractometer, equipped with a Ni-filtered Cu Kα radiation (0.15418 nm). The X-ray tube was operated at 40 kV and 40 mA. The data were collected in the 2θ range of 10–80°. The average crystallite sizes (D_{XRD}) were determined from XRD line broadening measurements using the Scherrer equation, $D_{XRD} = K\lambda/\beta\cos\theta$, where λ is the X-ray wavelength, θ is the diffraction angle, K is the particle shape factor, usually taken as 0.89, and β is full width at half maximum in radians.

Table 1
Copper oxide, cerium dioxide and zirconium dioxide loadings and crystalline size and BET surface area of the catalysts.

Catalysts	CuO loading mmol/100 m^2 γ-Al_2O_3	Ceria loading mmol/100 m^2 γ-Al_2O_3	Zirconia loading mmol/100 m^2 γ-Al_2O_3	Ce/Zr ratio	Crystallite size of γ-Al_2O_3 (nm)	Lattice constants (Å)[a]	Crystallite size of $Ce_xZr_{1-x}O_2$ (nm)[b]	BET surface area (m^2/g)
04CuZA	0.4	0	0.1	0:1	20.1	n.d.[c]	n.d.[c]	140.2
$04CuC_{0.33}Z_{0.67}A$	0.4	0.033	0.067	1:2	12.8	n.d.[c]	n.d.[c]	146.1
$04CuC_{0.5}Z_{0.5}A$	0.4	0.050	0.050	1:1	10.4	5.317	n.d.[c]	141.5
$04CuC_{0.67}Z_{0.33}A$	0.4	0.067	0.033	2:1	11.8	5.321	7.6	132.6
04CuCA	0.4	0.1	0	1:0	12.4	5.344	20.2	142.3

[a] Lattice constants are calculated from charateristic XRD peaks of $Ce_xZr_{1-x}O_2$ by Bragg's law.
[b] Crystallite size of $Ce_xZr_{1-x}O_2$ determined from the XRD diffraction peak by Scherrer equation.
[c] Not detected.

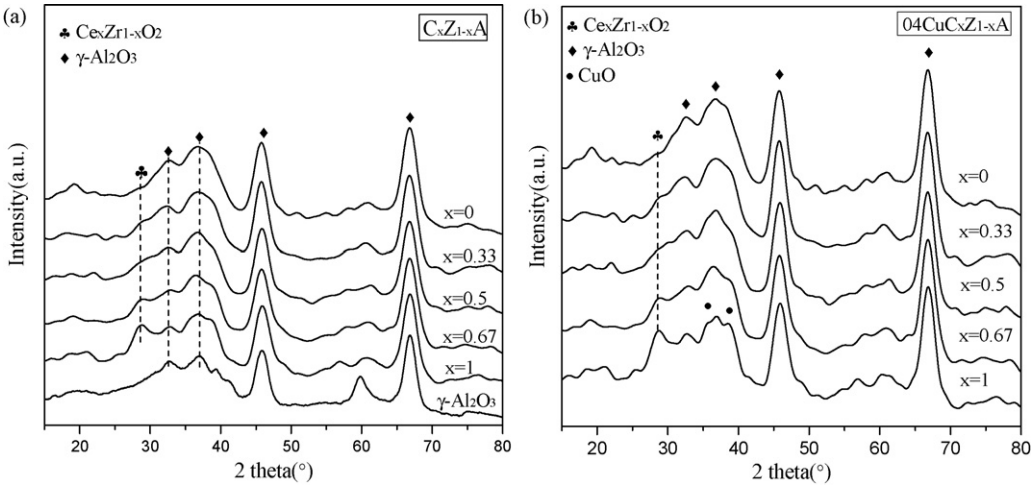

Fig. 1. The XRD patterns of (a) γ-Al_2O_3 and $C_xZ_{1-x}A$ (x = 0, 0.33, 0.5, 0.67, 1) supports; (b) $04CuC_xZ_{1-x}A$ (x = 0, 0.33, 0.5, 0.67, 1) catalysts.

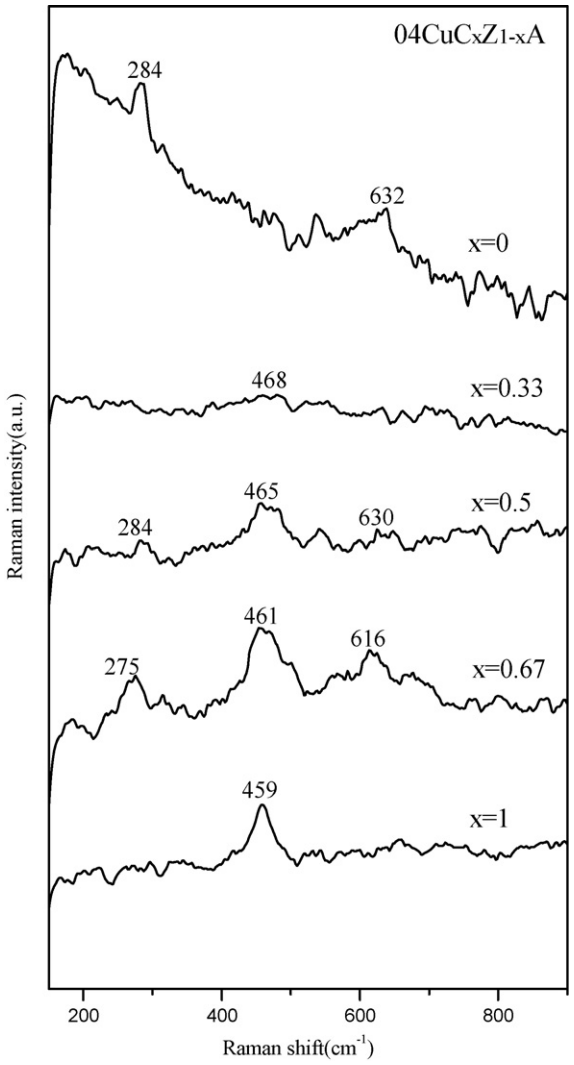

Fig. 2. The Raman spectra of $04CuC_xZ_{1-x}A$ (x = 0, 0.33, 0.5, 0.67, 1) catalysts.

2.2.3. Laser Raman spectroscopy (LRS)

LRS spectra were collected on a Jobin-Yvon (France-Japan) T64000 type Laser Raman spectroscopy using Ar^+ laser beam. The Raman spectra were recorded with an excitation wavelength at 514 nm and the laser power at 300 mW.

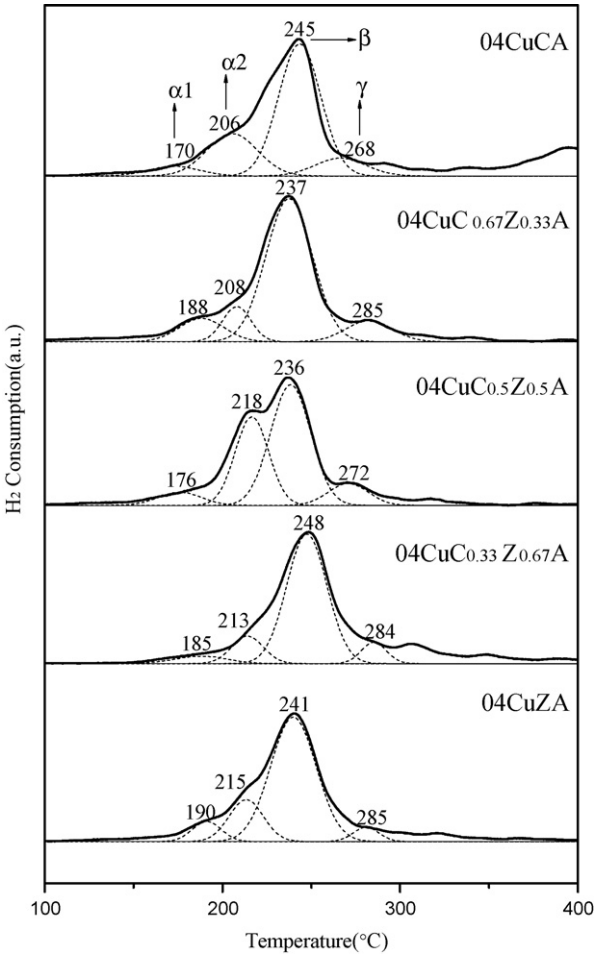

Fig. 3. The H_2-TPR profiles of $04CuC_xZ_{1-x}A$ (x = 0, 0.33, 0.5, 0.67, 1) catalysts.

2.2.4. H_2-temperature programmed reduction (H_2-TPR)

H_2-TPR experiments were performed in a quartz U-type reactor, and 50 mg sample was used for each measurement. Prior to the reduction, the catalyst was pretreated in N_2 stream at 100 °C for 1 h and then cooled to room temperature. After that, H_2–Ar mixture (7% H_2 by volume) was switched on, and the temperature increased gradually with a ramp of 10 °C/min. The H_2 consumption was monitored using a thermal conduction detector (TCD).

Table 2
TPR-fitting results of $04CuC_xZ_{1-x}A$ catalysts with different Ce/Zr molar ratios.

Catalysts	Temperature (°C)				Fraction of the total area (%)		
	α_1	α_2	β	γ	$\alpha(\alpha_1+\alpha_2)$	β	γ
04CuZA	190	215	241	285	24.3	68.5	7.2
$04CuC_{0.33}Z_{0.67}A$	185	213	248	284	16.1	66.7	17.2
$04CuC_{0.5}Z_{0.5}A$	176	218	236	272	37.4	51.2	11.4
$04CuC_{0.67}Z_{0.33}A$	188	208	237	285	20.9	68.2	10.8
04CuCA	170	206	245	268	27.4	57.9	14.6

2.2.5. *In situ Fourier transform-infrared spectroscopy (in situ FT-IR)*

In situ FT-IR experiments were carried out on a Nicolet 5700 equipped with a DTGS CaF_2 as detector running at a resolution of 4 cm^{-1}, and taking 32 scans for every spectrum. IR spectra for a mixed stream of NO–Ar (5% of NO by volume) and CO–Ar (10% of CO by volume) at a total flow rate of 10 ml/min were recorded from room temperature up to 300 °C. Approximately 15 mg sample in the form of self-supporting wafer mounted into a quarts IR cell, where they could be pretreated using N_2 at 100 °C for 1 h. The sample should be cooled to ambient temperature before each measurement, and then was exposed to the mixed stream of NO–CO for 30 min. Subsequently, a programmed temperature ramp was initiated at a rate of 10 °C/min from 25 to 300 °C. Finally, the catalysts were also exposed to NO–CO mixtures at 300 °C for about 30 min.

2.3. *Catalytic activity measurement*

The catalytic activity experiments were performed in a fixed bed, down flow, quartz reactor (length, 30 cm; inner diameter, 4 mm). The NO + CO reaction was investigated under steady state, involving a fixed feed with a gas composition of NO 5%, CO 10% and He 85% by volume as a carrier gas at a space velocity of 12,000 h^{-1}. For each measurement, 50 mg catalyst was pretreated in N_2 stream at 100 °C for 1 h and then be cooled to room temperature. After that, the valve gear was switched to the reaction gas. The activity measurements were conducted in ascending temperature mode, so that the light-off behavior could be recorded. Two volumes (length, 1.75 m; diameter, 3 mm) and thermal conduction detectors (T = 100 °C) were used for analyzing the production. Volume A was packed with 5A and 13X molecular sieves (40–60 mesh) for separating of O_2, N_2, NO and CO. Volume B was packed with Paropak Q for separating CO_2 and N_2O.

In addition, the rate of reaction was calculated by the equation:

$$\text{Rate} = \frac{pS_V\text{NO}\%}{RT} \times X_{\text{NO}} \quad (1)$$

where p is the atmospheric pressure, S_V the space velocity, NO% the NO volume fraction (5%), and X_{NO} is the NO conversion. The rate was expressed in $\mu mol_{NO}\ s^{-1}\ g_{cat}^{-1}$. Approximate TOFs at different temperatures were obtained by dividing the rate by the moles of copper oxide per gram catalyst. TOF was expressed in s^{-1}.

3. Results and discussion

3.1. *Characterization of catalysts*

Fig. 1 presented the XRD patterns of $C_xZ_{1-x}A$ supports and $04CuC_xZ_{1-x}A$ catalysts. It was seen that the main diffraction peak of crystalline ceria appeared at 28.5° for the catalyst modified by pure ceria [32]. In addition, extremely weak signals of CuO crystallites could be detected, indicating that copper oxide was well dispersed in all the catalysts. With the decreasing Ce/Zr ratio, the peak corresponding to cubic fluorite structure of ceria gradually weakened and even disappeared. Furthermore, the peak position

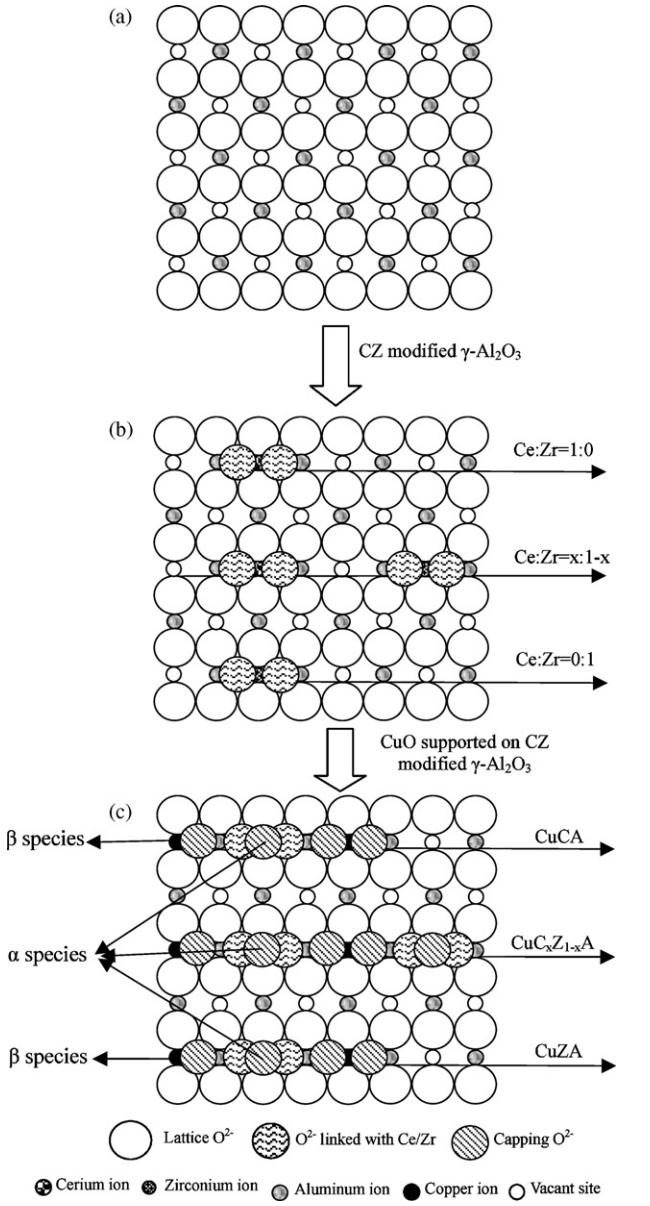

Fig. 4. A tentative model of the surface structure of (a) γ-Al_2O_3 support, (b) ceria or/and zirconia modified γ-Al_2O_3 and (c) incorporated copper species formed on $C_xZ_{1-x}A$.

of ceria (1 1 1) plane shifted from 28.5° to higher angle after the introduction of zirconia, and its lattice constant decreased correspondingly, as listed in Table 1. The lattice condensation should be resulted from the substitution of the large Ce^{4+} (0.92 Å) by small Zr^{4+} (0.79 Å), indicating that partial ceria–zirconia solid solution was formed. Similar phenomenon was also reported in previous literatures [33,34]. While for the 04CuZA catalyst, no characteristic peak associated with crystalline zirconia was observed, indicating that it was also highly dispersed on the surface of γ-Al_2O_3 support. Simultaneously, the surface areas of these $04CuC_xZ_{1-x}A$ catalysts slightly decreased in comparison with γ-Al_2O_3 support may due to pore blocking in the presence of crystalline particles. These above results suggested that the dispersion behaviors of ceria–zirconia were associated with the zirconium concentration in ceria lattice. According to our incorporation model [35], the surface vacant sites of γ-Al_2O_3 was preferentially occupied by the modifiers when ceria existed as rich phase at higher loading, and shielding effect was so remarkable due to the large ion radii of Ce^{4+} that might prevent

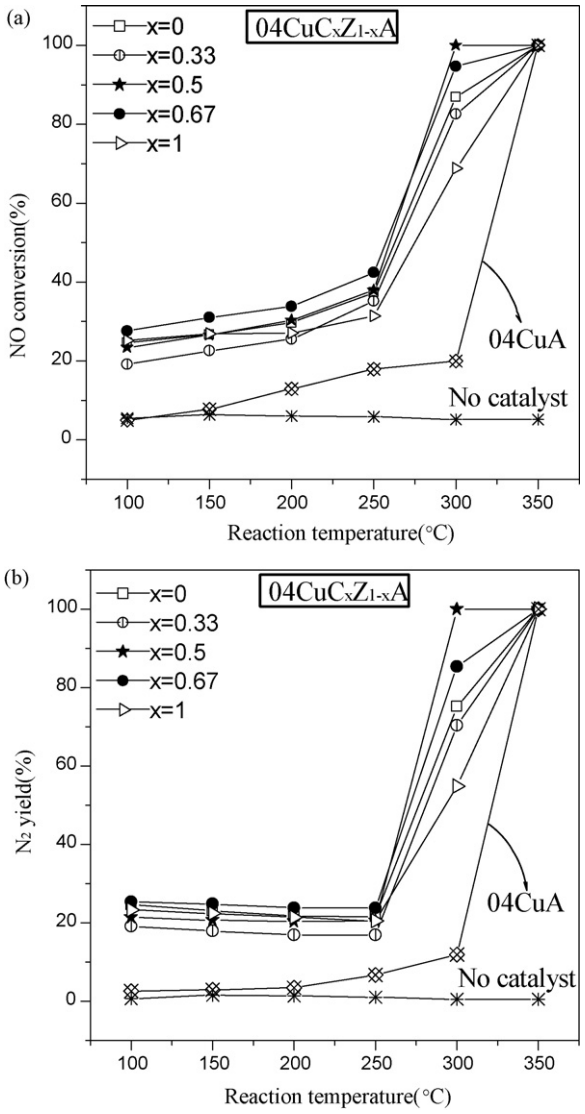

Fig. 5. (a) The NO conversion and (b) N_2 yield of 04CuA and $04CuC_xZ_{1-x}A$ (x = 0, 0.33, 0.5, 0.67, 1) catalysts. *Feed composition*: NO 5%, CO 10% and He 85%, S_V = 12,000 h^{-1}.

the distribution of ceria and copper species. Whereas in the case of zirconia as rich phase, the Zr^{4+} with small ion radii could obviously weaken the shielding effect, and thus these loading species could exist in well dispersion state.

Raman spectroscopy, a potential tool and sensitive to metal–oxygen arrangement and lattice defects, was performed to obtain additional structural information [36]. As shown in Fig. 2, the strong peak at 459 cm^{-1} for the 04CuCA sample was attributed to triply degenerate F_{2g} mode of the fluorite-type lattice, which can be viewed as a symmetric breathing mode of oxygen atoms around cerium ions [37]. For the 04CuZA sample, two bands at 284 and 632 cm^{-1} were the characteristic peaks related to the tetragonal zirconia [38]. Regarding the $04CuC_{0.67}Z_{0.33}A$ sample, the peak at 616 cm^{-1} corresponded to the nondegenerate Longitudinal Optical (LO) mode of ceria, which was liked to oxygen vacancies in the ceria lattice [39]. The appearance of another weak band at 275 cm^{-1} could be related to the displacement of oxygen atoms from their ideal fluorite lattice positions. In these $04CuC_xZ_{1-x}A$ ($0 < x < 1$) samples, two main features could be observed about the evolution of the Raman signals. Firstly, the strong peak at 461 cm^{-1} as well as two shoulders at 275 and 616 cm^{-1} shifted to higher wavenumber with decreasing of Ce/Zr ratio, which suggests enhancement

Table 3
Reaction rate and TOF data of NO + CO reaction over $04CuC_xZ_{1-x}A$ catalysts at 100, 200 and 300 °C. *Reaction conditions*: 50 mg catalysts, 5% NO–10% CO balanced with He, S_V = 12,000 h^{-1}.

Catalysts	Reaction rate ($\mu mol_{NO}\ s^{-1}\ g_{cat}^{-1}$)			TOF ($\times 10^{-3}\ s^{-1}$)[a]		
	100 °C	200 °C	300 °C	100 °C	200 °C	300 °C
04CuZA	1.66	1.98	5.84	2.85	3.41	10.0
$04CuC_{0.33}Z_{0.67}A$	1.29	1.71	5.55	2.22	2.95	9.6
$04CuC_{0.5}Z_{0.5}A$	1.57	2.03	6.72	2.71	3.52	11.6
$04CuC_{0.67}Z_{0.33}A$	1.86	2.28	6.36	3.19	3.92	10.9
04CuCA	1.69	1.82	4.62	2.90	3.13	7.9
04CuA	0.34	0.87	1.34	0.56	1.47	2.3

[a] The TOF here was calculated by the moles of NO converted per more of copper oxide in the whole catalyst per second.

in bond energies as a consequence of shorter M–O bond length as evidenced by lattice parameter estimation. This slight shift phenomenon was observed in several literatures similarly because of the introduction of doped zirconium ions [40,41]. On the other hand, the Raman intensity of these peaks decreased and broadened with decreasing of Ce/Zr ratio. In particular, when Ce/Zr ratio decrease to x = 0.33, there was only one broad lump at 468 cm^{-1}, and the peak at 630 and 284 cm^{-1} associated with oxygen vacancies have disappeared. As discussed elsewhere, the intensity of Raman signals depends on several factors including the grain size and morphology [42]. Combined with the XRD results in this work, the above observation should be associated with the decreasing of grain size of ceria–zirconia in the catalysts.

3.2. Effect of Ce/Zr ratio on the reducibility of catalysts

Fig. 3 depicted the TPR profiles for the $04CuC_xZ_{1-x}A$ catalysts. As reported in the literatures [16,20,43], two reduction peaks usually appeared on $CuO/\gamma\text{-}Al_2O_3$ system with variable copper oxide loadings, which were attributed to the well-dispersed and crystalline CuO, respectively. However, the TPR profiles for ceria- or/and zirconia-modified system became more complex. In the present study, for the sake of convenience, the reduction peaks in the temperature ranges of 170–190, 206–218, 237–248 and 268–285 °C were denoted as α_1, α_2, β, γ, respectively. According to our previous report [9], for the CuO/CeO_2 system, the dispersed copper species could incorporate into the cubic vacant sites of ceria and form a five-coordinated surface structure with the capping oxygen. While for the $CuO/\gamma\text{-}Al_2O_3$ catalyst, the dispersed copper species in the form of regular octahedral and defective octahedral structures exhibited different reducibility [43]. The asymmetrical five-coordinated structure was unstable compared to octahedral coordination, which led to the copper species more easily reduced. Thus these α peaks (including α_1 and α_2) at lower temperature were assigned to the reduction of highly dispersed CuO in close contact with ceria or/and zirconia on the surface of $\gamma\text{-}Al_2O_3$ [12,44,45]. The β peak corresponded to the reduction of CuO species dispersed on $\gamma\text{-}Al_2O_3$ surface was predominant among all peaks [9,20,43]. In addition, the γ peak at higher temperature was attributed to the reduction of small crystalline CuO, which was hardly observed in XRD patterns due to the detect limitation. It was concluded that copper species in proximity to ceria–zirconia were easily reduced because the addition of ceria and zirconia increased oxygen migration. As summarized in Table 2, the reduction temperature of these β peaks for $04CuC_{0.5}Z_{0.5}A$ and $04CuC_{0.67}Z_{0.33}A$ was lower than that of other samples. Considering the fraction of α peak over these $04CuC_xZ_{1-x}A$ ($0 < x < 1$) samples, an increase of Ce/Zr ratio resulted in the increase of α value, reached the maximum when x = 0.5, then followed by a decrease down to about 20%. Moreover, the fraction of α peak over $04CuC_{0.33}Z_{0.67}A$ was lower than that over others. These

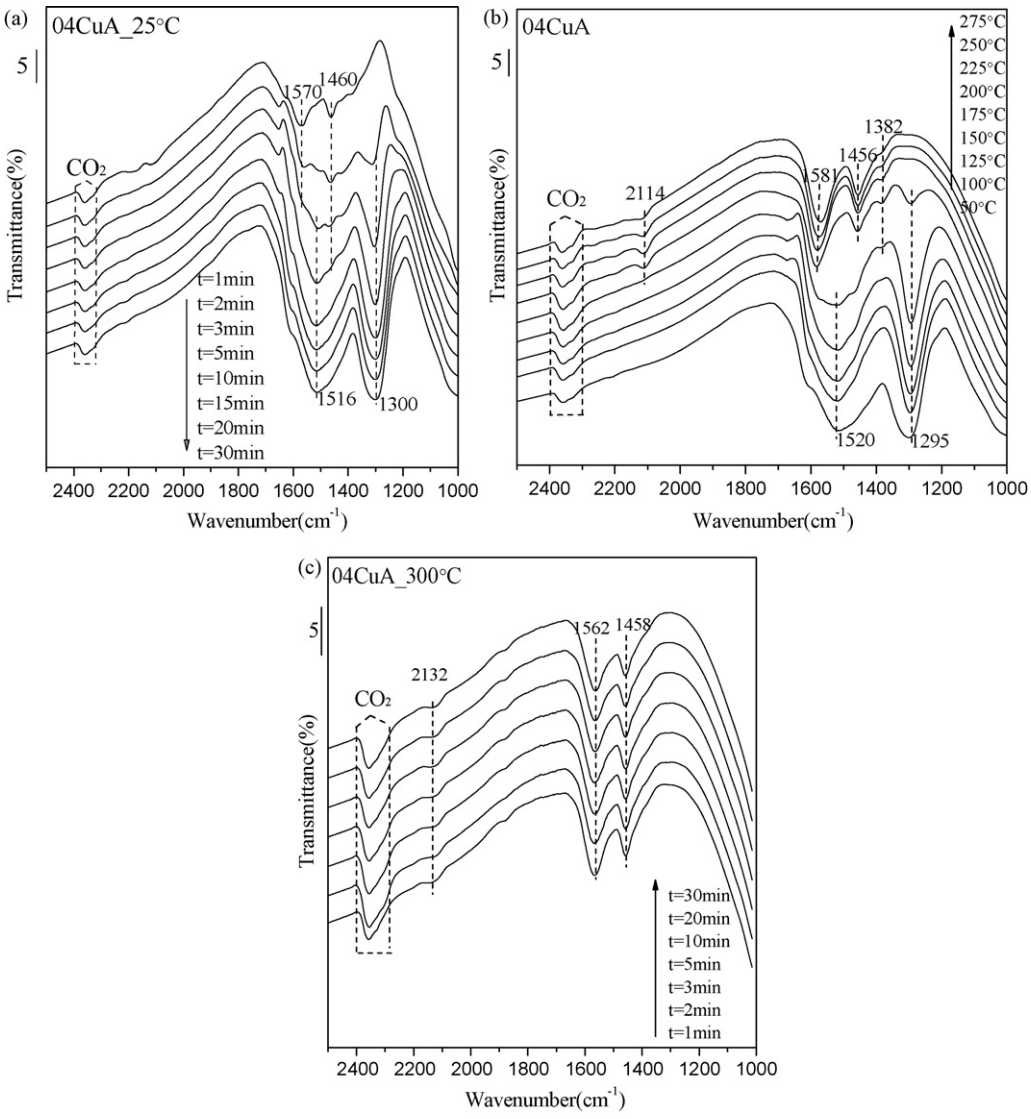

Fig. 6. In situ FT-IR spectra of 04CuA catalyst after exposure to NO (5%) and CO (10%). (a) 04CuA at 25 °C with different times; (b) 04CuA at different temperatures; (c) 04CuA at 300 °C with different times.

observations may due to different interaction between copper and ceria–zirconia [17]. From the above findings, it was suggested that ceria–zirconia mixed oxides with these molar ratios (2:1 and 1:1) readily promoted the reduction of copper species interacting with γ-Al_2O_3 [14]. In summary, the difference in the reducibility of copper oxide should be related to the different coordinate environments of copper species, which is due to different surface structures of ceria, zirconia, and alumina.

Due to the equal exposure possibilities of C- and *D*-layers on the preferentially (1 1 0) plane of γ-Al_2O_3 [9,35], we here only gave the *D*-layer of γ-Al_2O_3 (Fig. 4a). Then the preloaded ceria or/and zirconia only occupied some octahedral vacant sites of γ-Al_2O_3, accompanying with neighboring oxygen for charge compensation, whose existing state depended on the molar ratio of Ce/Zr (Fig. 4b). While the dispersed copper species were firstly combined with preloaded ceria or/and zirconia, and the others incorporated into the residual octahedral vacant sites of γ-Al_2O_3, as shown in Fig. 4c. Indubitably, these above-mentioned copper species (α and β) exhibited different reducibility due to the different coordinated environments. Considering the XRD and Raman results, the introduction of a proper amounts of zirconia into ceria lattice would lead to its lattice contraction and the increase of bulk defects, which could promote the oxygen mobility and enhanced the interaction between copper and $C_xZ_{1-x}A$ [25]. On the other hand, the formation of metal copper from the reduction of Cu^{2+} interacting with ceria or/and zirconia at low temperature may lead to the hydrogen spillover, which was from metal copper to surface incorporated copper species in the octahedral vacant sites of γ-Al_2O_3 [20,21]. Herein, the reduction temperature of the β peak in $04CuC_{0.5}Z_{0.5}A$ and $04CuC_{0.67}Z_{0.33}A$ samples decreased in comparison with others.

3.3. *Effect of Ce/Zr ratio on the activity of catalysts*

Fig. 5 showed the NO conversion and N_2 yield over these catalysts as a function of temperature. Notably, almost no activities were obtained when NO reduction by CO was operated without catalyst, and the addition of ceria–zirconia mixed oxides significantly improved the reactivity compared with the 04CuA sample. For these $04CuC_xZ_{1-x}A$ catalysts (Fig. 5a), it was found that NO conversion slightly increased from 100 to 250 °C. When the temperature was higher than 250 °C, the NO conversion increased dramatically and reached 100% at 350 °C. In addition, the catalyst performance was depended on the molar ratio of Ce/Zr in some extent. Overall, $04CuC_{0.67}Z_{0.33}A$ and $04CuC_{0.5}Z_{0.5}A$ gave the higher NO

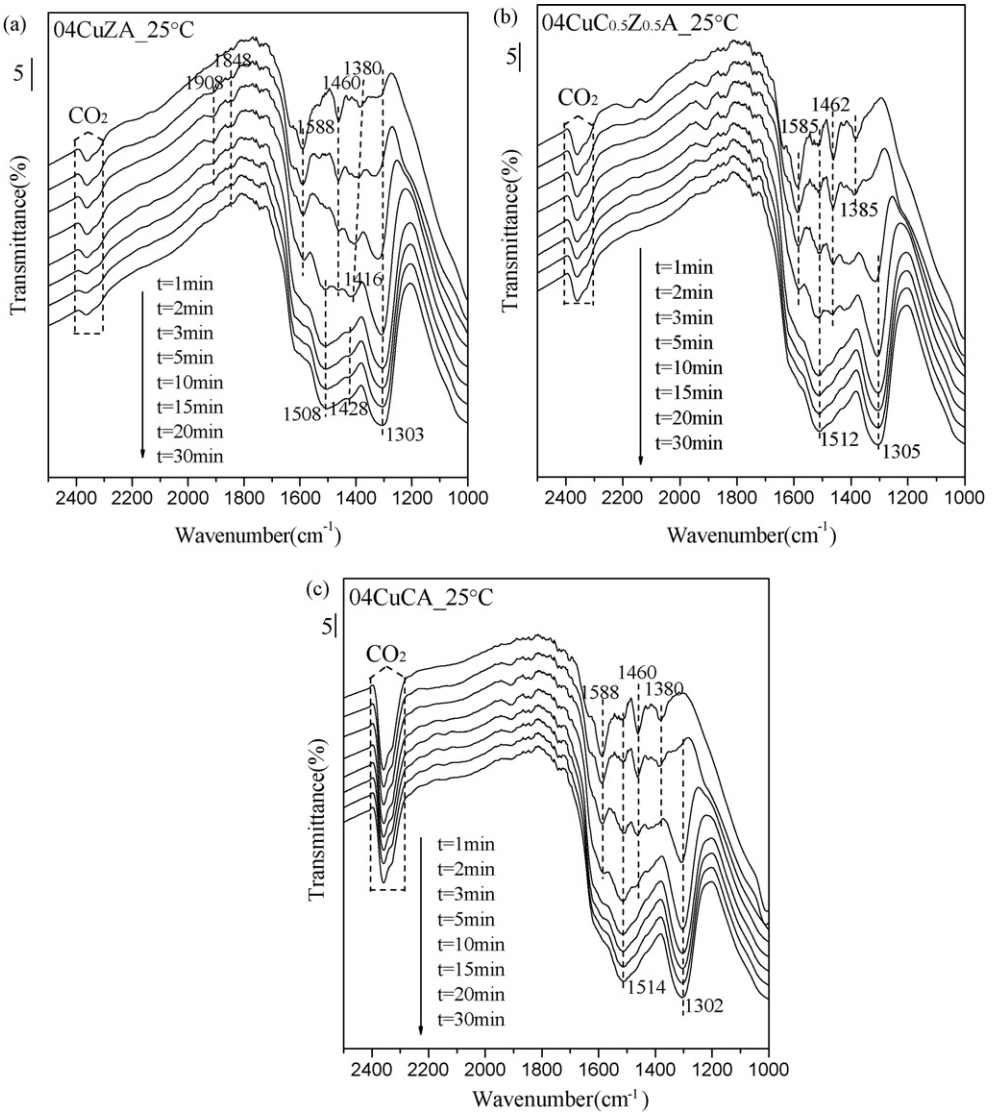

Fig. 7. In situ FT-IR spectra of the catalysts after exposure to NO (5%) and CO (10%) at 25 °C with different times. (a) 04CuZA; (b) $04CuC_{0.5}Z_{0.5}A$; (c) 04CuCA.

conversion than that over other samples. Especially at 300 °C, the difference in the activities was remarkable, following in this order: $04CuCA < 04CuC_{0.33}Z_{0.67}A < 04CuZA < 04CuC_{0.67}Z_{0.33}A < 04CuC_{0.5}Z_{0.5}A$, which should be related to the difference of interaction between copper species and ceria–zirconia modified γ-Al_2O_3. In view of N_2 yield over these catalysts (Fig. 5b), the remarkable difference could be observed below and above 250 °C. This might be resulted from the different active species at low and high temperatures, as evidenced in our published work [38,46]. Additionally, the N_2 yield followed the same order with NO conversion on $04CuC_xZ_{1-x}A$ catalysts at 300 °C.

The reaction rate and TOF data were also listed for the comparison of intrinsic activity in Table 3. The $04CuC_{0.67}Z_{0.33}A$ sample always showed the higher reaction rate. TOFs over $04CuC_{0.5}Z_{0.5}A$ and $04CuC_{0.67}Z_{0.33}A$ catalysts were about five times higher than that for 04CuA at 300 °C. The catalytic reduction of NO by CO over supported-metal catalyst was sensitive to the structure of supports, and associated with the reducibility of copper species. The interaction of metal–support could also be established to explain the difference in activity [5,9,13,15]. Based on all the above results, $04CuC_{0.5}Z_{0.5}A$ and $04CuC_{0.67}Z_{0.33}A$ samples possessed the strong reducibility, and displayed the better performance in activity correspondingly, which should be beneficial from the strong interaction among these components.

3.4. In situ FT-IR results of NO and CO co-adsorption with 04CuA catalyst

In situ FT-IR spectra of the co-adsorption of NO and CO over 04CuA catalyst at 25 °C was shown in Fig. 6a. After exposure to NO–CO mixtures, the bands at 1570 and 1460 cm^{-1} appeared immediately, which were attributed to the asymmetric and symmetric vibration of bidentate carbonates, respectively [47]. With the increase of exposure time, these species disappeared gradually and were replaced by a broad band at 1516 cm^{-1} (chelating nitrate species). Meanwhile, the band for nitrite species at 1300 cm^{-1} showed its maximum with prolonging the contact time. These results suggested that NO molecules were preferably and steadily adsorbed on the catalyst surface, and nitrate/nitrite species were formed at room temperature via adsorbed NO interacted with surface oxygen, which was possibly produced through the dissociation of hydroxyl on the catalyst surface. Moreover, the heating treatment resulted in the disappearance of the bands at about 1295 and 1520 cm^{-1} above 200 °C, indicating these nitrate/nitrite

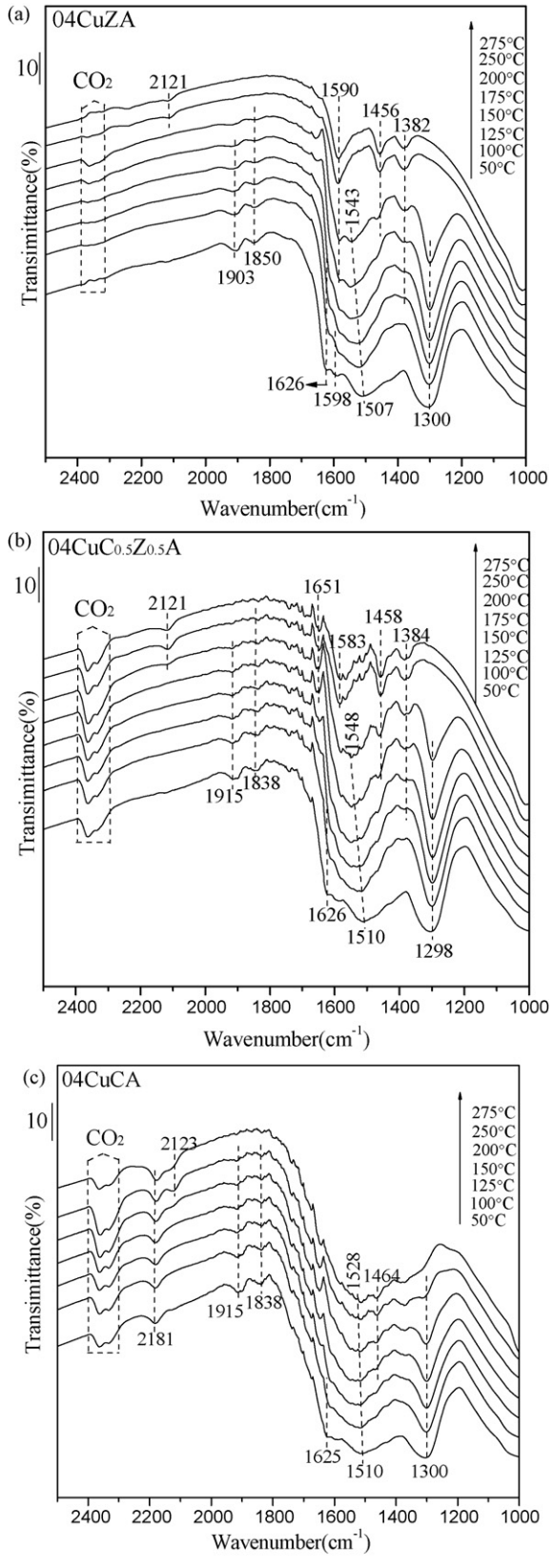

Fig. 8. In situ FT-IR spectra of the catalysts after exposure to NO (5%) and CO (10%) at different temperatures. (a) 04CuZA; (b) $04CuC_{0.5}Z_{0.5}A$; (c) 04CuCA.

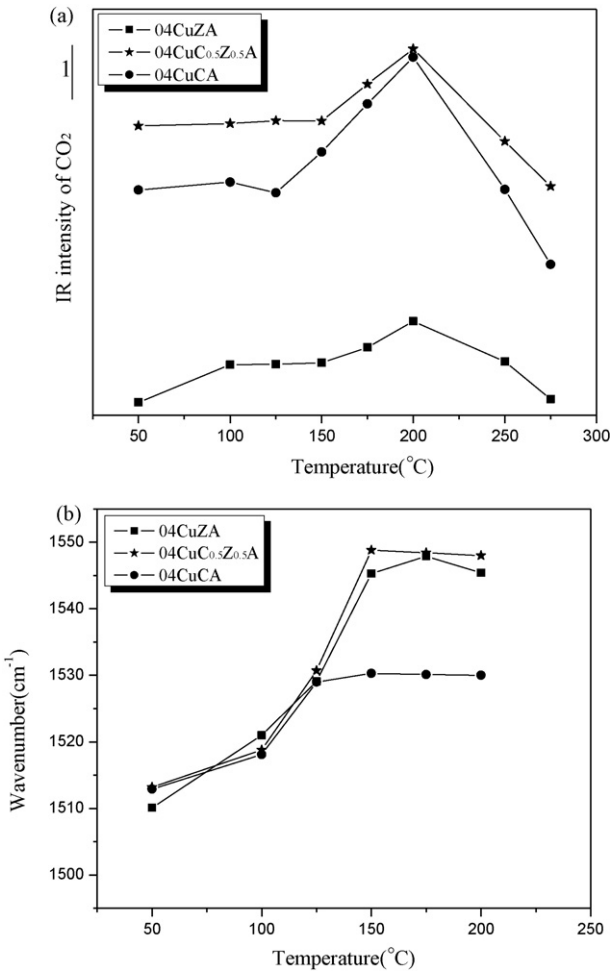

Fig. 9. (a) The relationship between the IR intensity of CO_2 and co-adsorption temperature and (b) the curves of the wavenumber of surface NO_x species as a function of temperature over $04CuC_xZ_{1-x}A$ ($x = 0$, 0.5, 1) catalysts.

species decomposed or reacted with adsorbed CO [48,49] (Fig. 6b). Instead, three new bands at 1581, 1456, and 1382 appeared at high temperature, which was assigned to the accumulation of other carbonate-like species due to excess CO [2,50]. In the higher wavenumber region, copper carbonyl (Cu^+-CO) appeared at 2114 cm^{-1} was observed above 200 °C, indicating that the reduced copper species worked at higher temperature [10]. Noteworthy, the bands at about 1562 and 1458 cm^{-1} associated with C-containing species were stable and unchanged independent of the exposure time when the temperature was fixed at 300 °C (Fig. 6c). It was deduced that these carbonate species covered with the catalyst surface may prevent the regeneration of the surface oxygen, which resulted in low activity.

3.5. Effect of Ce/Zr ratio on the adsorption behaviors of catalysts

Fig. 7 showed the FT-IR spectra of NO–CO reactants co-adsorption on 04CuZA, $04CuC_{0.5}Z_{0.5}A$ and 04CuCA catalysts at 25 °C as a function of exposure time. Taking 04CuZA as a sample (Fig. 7a), the bands at 1588 and 1460 cm^{-1} attributed to carbonate-like species dissolved after about 5 min and were substituted by new bands at 1508 and 1428 cm^{-1}. The band for linear nitrite species at 1303 cm^{-1} appeared immediately as exposed to the reactants, and was saturated after 5 min. Similar experimental results could be also observed over two other catalysts (Fig. 7b and c). These results suggested that the adsorbed nitrate/nitrite species

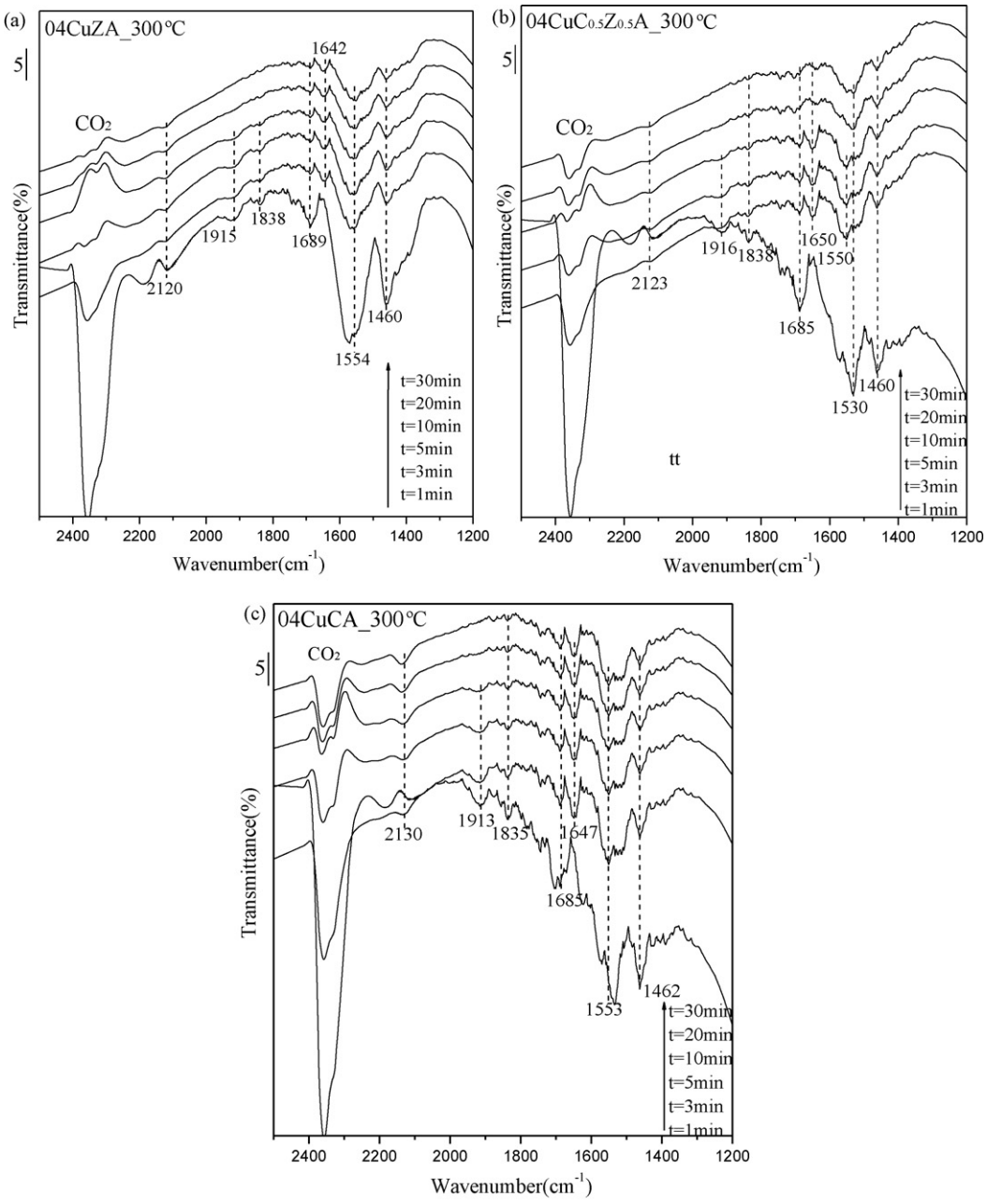

Fig. 10. In situ FT-IR spectra of the catalysts after exposure to NO (5%) and CO (10%) at 300 °C with different times. (a) 04CuZA; (b) $04CuC_{0.5}Z_{0.5}A$; (c) 04CuCA.

contacted with alumina were predominant and stable over these catalysts after purging by NO–CO mixtures for 30 min [47]. Moreover, their adsorption type and rate had no obvious relationship with the preloaded ceria or/and zirconia due to well dispersion.

Subsequently, great changes in the stability and type of adsorbed species occurred after increasing the temperature. In view of 04CuZA sample (Fig. 8a), the band for linear nitrite (1300 cm^{-1}) disappeared at 250 °C, while monodentate nitrate gradually shifted from 1507 to 1543 cm^{-1} and then completely vanished at 250 °C. Bidentate and bridging nitrates at 1598 and 1626 cm^{-1} were also rearranged into other forms due to thermal effects [2,38,46]. Simultaneously, three new bands at 1590, 1456 and 1382 cm^{-1} for surface carbonate-type species appeared at high temperature. Similar information was also obtained over $04CuC_{0.5}Z_{0.5}A$ sample (Fig. 8b). In the case of 04CuCA sample (Fig. 8c), some kinds of nitrite/nitrate species appeared at 1300, 1510 and 1625 cm^{-1} and kept relatively stable. This should be related to the character of strong basic O^{2-} of ceria. Differently, no new species appeared at high temperature over this pure ceria modified γ-Al_2O_3. These linear nitrites should be difficult converted to N_2 over all the catalysts below 250 °C, as evidenced by the N_2 yield results. Then the nitrite species become unstable and decomposed at high temperature accompanying with the increasing of catalytic activity. Analysis from the IR signals (1000–1700 cm^{-1}) over these three samples, the difference in the shape and wavenumber of these adsorbed carbonate- and nitrate-like species indicated that different crystal habit of ceria–zirconia might provide different adsorption sites, which was dependent on the molar ratio of Ce/Zr.

On the other hand, the distinction could also be found in the region of 1700–2500 cm^{-1}. For both pure ceria and zirconia modified catalysts, it was unambiguous that gaseous NO species physic-adsorbed on the surface of the catalyst displayed the bands at ~1838 and 1915 cm^{-1}, and completely disappeared above 250 °C due to thermal behavior [46,51]. Meanwhile, the copper carbonyl

(Cu^+-CO) was present at 2121 cm^{-1} [10], and carbonyl associated with cerium ions showed a characteristic band at 2181 cm^{-1}. These results suggested that different copper species operated at low and high temperature, which was related to the difference in the activity and N_2 yield. Whereas, Cu^+-CO appeared at 200 °C over $04CuC_{0.5}Z_{0.5}A$ sample, which indicated that ceria–zirconia mixed oxides (Ce/Zr = 1:1) facilitated the reduction of Cu^{2+} to Cu^+ species. This could be explained by the stronger interaction between ceria–zirconia and γ-Al_2O_3 than that of single CeO_2 and ZrO_2. This explanation was in agreement with the report that CeO_2–ZrO_2 mixed oxides could cover the Al_2O_3 surface as a monolayer and efficiently enhance the dispersion of copper species [2,52]. Those copper species preferentially interacted with CeO_2–ZrO_2 contributed the promotion effect on the NO reduction.

Fig. 9a displayed the evolution of CO_2 IR intensity as a function of reaction temperature over $04CuC_xZ_{1-x}A$ ($x = 0, 0.5, 1$) catalysts. Notably, significant differences distinguished from the IR intensity of CO_2 over these catalysts reflected that the amount of product for NO + CO reaction was depended on Ce/Zr ratio. In addition, For $04CuC_{0.5}Z_{0.5}A$ catalyst, surface NO_x species gradually blue shifted to higher wavenumber than those of 04CuZA and 04CuCA above 150 °C (Fig. 9b), which may be due to adsorbed NO easily interacting with active oxygen generated from the surface of ceria–zirconia via $NO_{ad} + x - 1[O]_{actived} \rightarrow NO_x$ [2].

In situ FT-IR was also performed on NO/CO co-adsorption with $04CuC_xZ_{1-x}A$ ($x = 0, 0.5, 1$) catalysts at 300 °C as a function of time, as shown in Fig. 10. At the initial stage, the reaction quickly took place as large amount of CO_2 formation. Accompany with the prolonging time, the adsorbed NO species disappeared due to the formation of other N-containing species or decomposed [38]. Correspondingly, the resultant surface carbonates and bicarbonates species dominated the catalyst surface, which should be related to the relative alkalescency of γ-Al_2O_3 and excess CO. Interestingly, the Cu^+ carboxyl over these three catalysts showed the difference in wavenumber. This was resulted from the different interaction among the copper, ceria–zirconia and γ-Al_2O_3, which determined the coordination environment of copper species.

4. Conclusion

The present work explored the effects of Ce/Zr molar ratio (low loading) on the physicochemical properties of $CuO/Ce_xZr_{1-x}O_2/\gamma$-$Al_2O_3$ catalysts. It was found that copper oxide dispersed on $Ce_xZr_{1-x}O_2/\gamma$-Al_2O_3 exhibited the different reducibility, which corresponded to the copper species with different coordinated environments. Furthermore, the ceria-rich modified catalyst showed the higher activity and TOF towards NO reduction, as compared with the pure ceria and zirconia-rich ones. These were resulted from the difference in the interaction among the copper, ceria–zirconia and γ-Al_2O_3 support.

Additionally, FT-IR results suggested that the preloaded ceria or/and zirconia with low loading had no obvious influence on the adsorption type and rate of NO and CO. Simultaneously, the stability of these N- and C-containing intermediates contacted with alumina was influenced by the modified Ce/Zr molar ratio. The surface carbonates dominated the reaction process above 250 °C due to excess CO. Different copper species worked at low and high temperature region, and the reduced copper species (Cu^+) played an important role in enhancing the activity at high temperature.

Acknowledgements

The financial supports of the National Natural Science Foundation of China (Nos. 20873060, 20973091), the Project of Jiangsu innovation talent (BK2008001) and the National 973 Program of China (No. 2010CB732300) are gratefully acknowledged.

References

[1] M. Fernández-García, A. Martínez-Arias, A. Iglesias-Juez, A.B. Hungría, J.A. Anderson, J.C. Conesa, J. Soria, J. Catal. 214 (2003) 220–233.
[2] R. Di Monte, J. Kašpar, P. Fornasiero, M. Graziani, C. Pazé, G. Gubitosa, Inorg. Chim. Acta 334 (2002) 318–326.
[3] R. Pérez-Hernández, F. Aguilar, A. Gómez-Cortés, G. Díaz, Catal. Today 107–108 (2005) 175–180.
[4] P. Granger, C. Dujardin, J.F. Paul, G. Leclercq, J. Mol. Catal. A: Chem. 228 (2005) 241–253.
[5] D.R. Rainer, S.M. Vesecky, M. Koranne, W.S. Oh, D.W. Goodman, J. Catal. 167 (1997) 234–241.
[6] K.A. Almusaiteer, S.S.C. Chuang, C.D. Tan, J. Catal. 189 (2000) 247–252.
[7] M. Shelef, K. Otto, H.S. Gandhi, J. Catal. 12 (1968) 361–375.
[8] X.Y. Jiang, L.P. Lou, G.H. Ding, Y.X. Chen, X.M. Zheng, J. Mater. Sci. 39 (2004) 4663–4667.
[9] Y.H. Hu, L. Dong, M.M. Shen, D. Liu, J. Wang, W.P. Ding, Y. Chen, Appl. Catal. B: Environ. 31 (2001) 61–69.
[10] A.B. Hungría, A. Iglesias-Juez, A. Martínez-Arias, M. Fernández-García, J.A. Anderson, J.C. Conesa, J. Soria, J. Catal. 206 (2002) 281–294.
[11] H.Y. Zhu, M.M. Shen, F. Gao, Y. Kong, L. Dong, Y. Chen, C. Jian, Z. Liu, Catal. Commun. 5 (2004) 453–456.
[12] X.Y. Jiang, L.P. Lou, Y.X. Chen, X.M. Zheng, J. Mol. Catal. A: Chem. 197 (2003) 193–205.
[13] P.W. Park, J.S. Ledford, Appl. Catal. B: Environ. 15 (1998) 221–231.
[14] Y.H. Hu, L. Dong, J. Wang, W.P. Ding, Y. Chen, J. Mol. Catal. A: Chem. 162 (2000) 307–316.
[15] M. Khristova, B. Ivanov, I. Spassova, T. Spassov, Catal. Lett. 119 (2007) 79–86.
[16] P.O. Larsson, A. Andersson, Appl. Catal. B: Environ. 24 (2000) 175–192.
[17] A. Martínez-Arias, R. Cataluña, J.C. Conesa, J. Soria, J. Phys. Chem. B 102 (1998) 809–817.
[18] M. Fernández-García, E. Gómez Rebollo, A. Guerrero Ruiz, J.C. Conesa, J. Soria, J. Catal. 172 (1997) 146–159.
[19] X.Y. Jiang, R.X. Zhou, P. Pan, B. Zhu, X.X. Yuan, X.M. Zheng, Appl. Catal. A: Gen. 150 (1997) 131–141.
[20] W.P. Dow, Y.P. Wang, T.J. Huang, Appl. Catal. A: Gen. 190 (2000) 25–34.
[21] J.B. Wang, W.H. Shih, T.J. Huang, Appl. Catal. A: Gen. 203 (2000) 191–199.
[22] B. Lindström, L.J. Pettersson, P.G. Menon, Appl. Catal. A: Gen. 234 (2002) 111–125.
[23] G.V. Sagar, P.V. Ramana Rao, C.S. Srikanth, K.V.R. Chary, J. Phys. Chem. B 110 (2006) 13881–13888.
[24] I. Heo, J.W. Choung, P.S. Kim, I.S. Nam, Y.I. Song, C.B. In, G.K. Yeo, Appl. Catal. B: Environ. 92 (2009) 114–125.
[25] S. Letichevskya, C.A. Tellez, R.R. de Avillez, M.I.P. da Silva, Appl. Catal. B: Environ. 58 (2005) 203–210.
[26] H.O. Zhu, J.R. Kim, S.K. Ihm, Appl. Catal. B: Environ. 86 (2009) 87–92.
[27] J.R. Kim, W.J. Myeong, S.K. Ihm, Appl. Catal. B: Environ. 71 (2007) 57–63.
[28] R. Di Monte, P. Fornasiero, J. Kašpar, M. Graziani, J.M. Gatica, S. Bernal, A. Gómez-Herrero, Chem. Commun. (2000) 2167–2168.
[29] A. Martínez-Arias, M. Fernández-García, A. Iglesias-Juez, A.B. Hungría, J.A. Anderson, J.C. Conesa, J. Soria, Appl. Catal. B: Environ. 31 (2001) 51–60.
[30] M. Fernández-García, A. Martínez-Arias, A. Iglesias-Juez, C. Belver, A.B. Hungría, J.C. Conesa, J. Soria, J. Catal. 194 (2000) 385–392.
[31] L. Dong, Y. Chen, Chin. J. Inorg. Chem. 16 (2000) 250–260.
[32] H.Q. Wan, D. Li, Y. Dai, Y.H. Hu, Y.H. Zhang, L.J. Liu, B. Zhao, B. Liu, K.Q. Sun, L. Dong, Y. Chen, Appl. Catal. A: Gen. 360 (2009) 26–32.
[33] M. Ferńandez-García, A. Martínez-Arias, A. Iglesias-Juez, A.B. Hungría, J.A. Anderson, J.C. Conesa, J. Soria, Appl. Catal. B: Environ. 31 (2001) 39–50.
[34] J.R. Kim, W.J. Myeong, S.K. Ihm, J. Catal. 263 (2009) 123–133.
[35] Y. Chen, L.F. Zhang, Catal. Lett. 12 (1992) 51–62.
[36] H. Knözinger, G. Mestl, Top. Catal. 8 (1999) 45–55.
[37] H. Vidal, J. Kašpar, M. Pijolat, G. Colon, S. Bernal, A. Cordón, V. Perrichon, F. Fally, Appl. Catal. B: Environ. 30 (2001) 75–85.
[38] L.J. Liu, B. Liu, L.H. Dong, J. Zhu, H.Q. Wan, K.Q. Sun, B. Zhao, H.Y. Zhu, L. Dong, Y. Chen, Appl. Catal. B: Environ. 90 (2009) 578–586.
[39] B.M. Reddy, P. Bharali, P. Saika, S.E. Park, M.W.E. Vanden Berg, M. Muhler, W. Grünert, J. Phys. Chem. C 112 (2008) 11729–11737.
[40] R. Si, Y.W. Zhang, S.J. Li, B.X. Lin, C.H. Yan, J. Phys. Chem. B 108 (2004) 12481–12488.
[41] B.M. Reddy, P. Saika, P. Bharali, Catal. Surv. Asia 12 (2008) 214–228.
[42] J.E. Spanier, R.D. Robinson, F. Zhang, S.W. Chan, I.P. Herman, Phys. Rev. B 64 (2001) 245407.
[43] H.Q. Wan, Z. Wang, J. Zhu, X.W. Li, B. Liu, F. Gao, L. Dong, Y. Chen, Appl. Catal. B: Environ. 79 (2008) 254–261.
[44] C.Y. Shiau, M.W. Ma, C.S. Chuang, Appl. Catal. A: Gen. 301 (2006) 89–95.
[45] M. Ferńandez-García, I. Rodríguez-Ramos, P. Ferreira-Aparicio, A. Guerrero-Ruiz, J. Catal. 178 (1998) 253–263.
[46] L.J. Liu, Y. Chen, L.H. Dong, J. Zhu, H.Q. Wan, B. Liu, B. Zhao, H.Y. Zhu, K.Q. Sun, L. Dong, Y. Chen, Appl. Catal. B: Environ. 90 (2009) 105–114.

[47] K.A. Almusaiteer, S.S.C. Chuang, J. Phys. Chem. B 104 (2000) 2265–2272.
[48] I. Spassova, M. Khristova, D. Panayotov, D. Mehandjiev, J. Catal. 185 (1999) 43–57.
[49] N.B. Stankova, M.S. Khristova, D.R. Mehandjiev, J. Colloid Interf. Sci. 241 (2001) 439–447.
[50] M. Fernández-García, A. Martínez-Arias, C. Belver, J.A. Anderson, J.C. Conesa, J. Soria, J. Catal. 190 (2000) 387–395.
[51] Y. Chi, S.S.C. Chuang, J. Catal. 190 (2000) 75–91.
[52] T. Horiuchi, Y. Teshima, T. Osaki, T. Sugiyama, K. Suzuki, T. Mori, Catal. Lett. 62 (1999) 107–111.